

Thermal performance of coupled cool roof and cool façade: Experimental monitoring and analytical optimization procedure



A.L. Pisello^{a,*}, V.L. Castaldo^b, C. Piselli^b, C. Fabiani^b, F. Cotana^a

^a Department of Engineering – University of Perugia, Via Duranti 63, 06125 Perugia, Italy

^b CIRIAF – Interuniversity Research Center on Pollution and Environment “Mauro Felli”, Via Duranti 67, 06125 Perugia, Italy

ARTICLE INFO

Article history:

Received 30 September 2016

Received in revised form 23 March 2017

Accepted 20 April 2017

Available online 23 April 2017

Keywords:

Cool roof

Cool façade

Continuous monitoring

Building thermal-energy performance

Sensitivity analysis

Analytical procedure

ABSTRACT

While UHI mitigation potential of cool roofs has been deeply investigated compared to cool façades, still not sufficient research effort has been dedicated to quantify the benefits of combined cool building products.

The present work evaluates the thermal performance of an innovative cool roofing membrane and a cool façade painting applied on a prototype building. Moreover, an analytical procedure able to predict the cool coating thermal performance is elaborated. Such methodology can be used to determine the passive cooling potential of each product as a separate envelope component and as a combination. To this twofold aim, a preliminary in-field monitoring is developed. Therefore, a sensitivity analysis is performed to evaluate the separate and combined passive cooling contributions of the roof and the differently oriented façades. Finally, the analytical procedure is developed to define external surface temperature profiles able to predict the building coating thermal performance by minimizing the number of temperature measurements.

Results show the major contribution of cool roof membrane in reducing indoor operative temperature. Nevertheless, a non-negligible cooling effect in terms of outdoor surface temperature is imputable to the South cool façade. Moreover, the analytical model shows an acceptable accuracy in representing the behavior of the building coating.

© 2017 Elsevier B.V. All rights reserved.

1. Introduction and motivation

Urban Heat Island (UHI) is a well acknowledged local urban microclimate phenomenon [1] characterized by higher temperatures in urban areas compared to the surrounding suburban and rural areas [2]. It is due to multiple factors, such as solar radiation trapping and wind shelters caused by urban street canyon geometry, urban greenhouse effect, diminution of evaporative surfaces and storage of sensible heat in the city fabric, and released anthropogenic heat [3]. Although mitigating the heating energy requirement in winter, UHI increases the cooling energy demand in summer. Therefore, in last decades the contribution of air conditioning in buildings energy consumption has been growing [4].

Several studies focused on the development of techniques for mitigating the UHI phenomenon and therefore for improving the quality of the local urban environment, such as smart materials

with high optic-thermal performances [5], increased urban green areas [6], solar shading of urban surfaces [7], cool building coating materials [8]. The potential of such cool materials has been widely investigated in roof applications, while their capability in mitigating UHI when applied in building façades is still not well acknowledged [9]. Findings confirmed the potential of this technique in southern European climatic conditions. Considering cool roof applicability in cold climates, Mastrapostoli et al. [10] observed a decrease of 73% for cooling, with negligible heating penalties, as a result of the application of a cool roof fluorocarbon coating for an industrial building in Oss, Netherlands. In order to compare the performance of such innovative materials under different boundary conditions, dedicated building prototypes have been often used. For instance, Doya et al. [11] employed reduced-scale building prototypes in a typical urban canyon configuration to assess the thermal effects of cool façade paints on both building and outdoor environment. Using five dedicated test cells, Revel et al. [12] monitored the thermal performance of cool coloured ceramic tiles, acrylic paints and bituminous membranes for both roof and walls [13]. However, previous studies demonstrated not only the considerable mitigation effect of cool surfaces with respect to the urban environ-

* Corresponding author.

E-mail addresses: anna.pisello@unipg.it, pisello@crbnet.it (A.L. Pisello), castaldo@crbnet.it (V.L. Castaldo).

Nomenclature

S	Standard scenario
CR	Cool Roof scenario
CR + CSF	Cool Roof and Cool South Façade scenario
CE	Cool Envelope coating scenario
SF, NF, EF, WF	South façade, North façade, East façade, and West façade, respectively
IP	Input parameter
OP	Output parameter
SC	Sensitivity coefficient
T_{op}	Indoor operative temperature
T_{out}	Outdoor dry-bulb temperature
R^*	Building coating equivalent reflectance
R_{solar}	Solar reflectance
A	Surface area
VF	Surface view factor to the sky
φ	Surface tilt angle from horizontal
T_s, T_n, T_e, T_w, T_r	Surface temperatures of the differently oriented building surfaces, i.e. South, North, East, West, and roof, respectively
T_j^*	Approximated building coating surface temperature, with j being the five different surface orientations considered, i.e. j = East (E), West (W), South (S), North (N), roof (R)
T_{skin}^*	Approximated building coating surface temperature
e_i, w_i, s_i, n_i, r_i	Fitting parameters for each specific envelope component surface, with i being the number of the selected day, varying between 1 and 5
a_i, b_i, c_i	Fourier series fitting coefficients for the $T_{fj}, T_s, T_n, T_e, T_w, T_r$
$E_{1...8}$	Parameters obtained from the fitting procedure by using the Fourier of 3rd order for the additional monitored summer day selected
$z_{lim,1}$ and $z_{lim,2}$	Boundary solar azimuth angles (upper and lower limit, respectively)
h_{lim}	Boundary solar altitude angle
L_e, L_s	East and South wall length
r_{base}	Semi-diagonal of the building base
r_h	Maximum distance between the center of the case study building and its roof

ment, but showed also how the locally thermally enhanced urban environment itself can mutually influence the thermal-energy performance of the urban context characterized by such materials. Santamouris et al. [14] showed how the buildings thermal performance can significantly benefit from local refurbishment strategies, i.e. application of innovative sustainable and high-performance materials, in different climate conditions and projections. Moreover, it was proved that cool coatings providing high reflectivity of solar radiation on the materials used on pavements and walls inside an urban context are able to decrease surface temperature up to 7–8 °C at ground level and ambient air temperature up to 1 °C. The reduction of absorbed solar radiation leads therefore to considerable energy saving and thermal comfort conditions in cities, and represent a good countermeasure to the heat island effect [15]. In fact, pavements and buildings surfaces, i.e. roofs and walls, represent a huge fraction of the urban areas and significantly contribute to the development of heat island in cities. Cool materials presenting lower surface temperature and reduced sensible heat flux to the atmosphere appear to be one of the most important proposed mitigation solutions [16].

In this panorama, this work has a twofold objective. Firstly, the thermal benefits deriving from the application of two innovative cool coating solutions, i.e. a cool roof membrane and façade painting, able to mitigate local environmental conditions are evaluated both as separate and combined solutions. To this aim, the in-field continuous monitoring of their main thermal and optical parameters is carried out when applied on a dedicated test-room building situated in central Italy. Secondly, an analytical tool able to predict the thermal performance of the cool building coating in terms of surface temperature of the differently oriented surfaces (i.e. roof and façades), without needing the experimental measurements for all of them, is implemented. The procedure for the development of the analytical model is based on the experimental data. The tool is aimed at minimizing the need for experimental measurements, by defining how many and which building external surfaces must be monitored to obtain an accurate estimation of the whole building coating thermal performance. The question is indeed if the external surface temperature of the whole building coating can be described by using only the experimental data referred, for instance, to two single building walls, without neglecting the impact of the orientation and by computing the inaccuracies.

Building upon previous research works, in this paper an experimental and an analytical approach are combined with the twofold purpose of:

- [(ii)]
- (i) assess the separate and combined thermal benefit deriving from the application of cool coatings on differently oriented building envelope surfaces and
- (ii) define a tool able to predict the building external coating thermal performance with the minimum effort in terms of experimental monitoring campaign.

In order to pursue the first goal, a sensitivity analysis is carried out to:

- [(ii)]
- (i) compare the effects of the two combined envelope strategies, i.e. cool roof and cool façade, and
- (ii) to determine the impact of the cool wall painting application depending on the different façade orientation.

On the other hand, to achieve the second goal, an analytical methodology is implemented in order to:

- [(ii)]
- (i) define a univocal surface temperature function representative of the whole case study building coating thermal behaviour, able to reproduce the difference between the standard and cool configuration of the building, and
- (ii) predict the building external coating thermal performance based on the lowest possible number of experimental sensors with specific position on the building external surfaces.

Therefore, this study aims at bridging the gap between building analytical modelling and the need for a lot of experimental measurements as input data. In fact, models allowing to predict buildings behaviour are useless if time-consuming and expensive experimental monitoring campaigns are needed for validation purposes.

2. Materials and methods

2.1. Methodology

The methodology implemented in this work is mainly based on (i) continuous monitoring of outdoor and indoor microclimate parameters in a prototype building, i.e. test-room, (ii) data and sensitivity analysis of the cool coatings performance, and (iii) development of an analytical procedure able to produce a case-

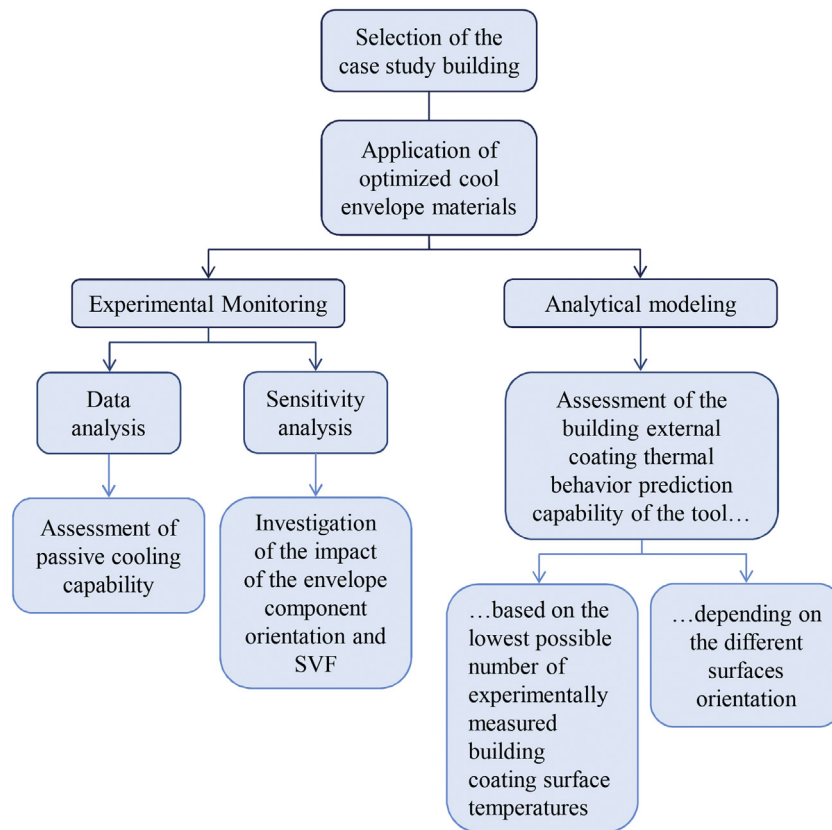


Fig. 1. Flowchart of the work methodology.

specific model that predicts the building external coating thermal behaviour with reduced experimental data required.

The methodology path is summarized in Fig. 1.

2.2. Experimental continuous monitoring

In order to compare the environmental thermal benefits of the cool roof membrane and cool façade painting, the two innovative cool coating solutions were applied on the roof and the differently oriented walls, respectively, of a dedicated prototype case study building, i.e. test-room. The building is located inside the university campus in Perugia, in central Italy. The in-situ continuous monitoring of the thermal performance of the proposed solutions was carried out during summer 2014 and 2015. The main indoor/outdoor thermal parameters and the roof albedo were monitored. In particular, the surface temperatures of all the differently oriented building façades were monitored in order to highlight the positive thermal mitigation effect of the application of the cool wall painting depending on the surface orientation.

Firstly, the case study building with non-cool coating materials, i.e. bitumen membrane and red-coloured painting, was monitored as base case scenario. Secondly, the cool membrane was applied on the test-room roof, in order to assess the specific contribution of the cool roof to the thermal performance of the test-room in summer conditions. Thereafter, the cool painting was applied in the differently oriented façades, i.e. South, North, East, and West facing façades of the same case study prototype building, by painting one façade at a time. In this way, the performance of the coupled solutions is analysed, and the impact of the different wall orientation on the passive cooling effect of the reflective painting is evaluated.

The monitored data were subsequently post-processed to compare the thermal effect of the two cool solutions. In particular, a sensitivity analysis was performed to understand the coupled

cooling contribution of the cool roof and the differently oriented cool façades. In detail, the following different scenarios for the case study building envelope were identified:

[•]

- Cool Roof scenario (CR): the innovative cool roof membrane is applied over the existing membrane of the case study building Standard scenario.
- Cool Roof and Cool South Façade scenario (CR + CSF): the further innovative cool façade painting is applied on the South-facing façade of the case study building Cool Roof scenario.
- Cool Envelope coating scenario (CE) including cool roof: the innovative cool façade painting is applied on all the further remaining building façades of the case study building Cool Roof and Cool South Façade scenario, i.e. East, West, and North façade.

In detail, the cool roofing membrane consists of a polyurethane-based waterproof liquid white membrane with high elasticity. The cooling potential of such membrane was optimized through iterative laboratory and in-field tests by increasing specific components such as the titanium dioxide (TiO₂) and hollow ceramic microspheres percentage in order to obtain the highest achievable solar reflectance capability [17]. The final optimized membrane, characterized by a R_{solar} value (measured in-lab) equal to 0.83, presented almost 12% of TiO₂ and 4% of hollow ceramic microspheres.

The proposed cool painting for building façade applications consists of an almost white non-organic painting, mainly composed by potassium silicate with small percentage of resin. It is characterized by high vapor permeability. The painting was optimized by increasing TiO₂ and hollow ceramic microspheres percentage through the same in-lab iterative process used for the cool roofing membrane. The most performing combination, i.e. the painting with the highest R_{solar} value (measured in-lab) equal to 0.81, was found to be again with 12% of TiO₂ and 4% of hollow ceramic microspheres.



Fig. 2. Pyranometer used in the experimental campaign to measure the radiation reflected from the roof.

The innovation of such proposed highly reflective materials consists mainly in their high-performance based on low-cost preliminary optimization process carried out by the same authors in-lab and in-field [17,18]. Moreover, during the monitoring campaign in-field albedo measurement of the cool and standard roof solutions was carried out when applied over the test-room. In details, the analysis of the optical properties of the two roof coating solutions was carried out by comparing the in-field mid-day albedo measured during summer 2014. The experimental campaign was performed according to the operative guidelines reported in the ASTM E1918 (2006) Standard Test Method [19] by means of two pyranometers facing opposite direction: the one positioned on the top of the test-room roof facing the roof coating able to measure the reflected solar radiation from the roof (Fig. 2) and the other located on the meteorological station able to measure the incoming global solar radiation [20]. Therefore, the calculation of the ratio between the reflected radiation and the incoming solar radiation as measured by the pyranometers, i.e. the albedo, was carried out for each membrane. More in detail, the two pyranometers are ISO 9060 [21] CL2 thermopile global radiometers with a spectral range of 305/2800 nm, a measurement range $<2000 \text{ W/m}^2$, and an output sensitivity of 12.27 and 13.03 mV/Wm^2 , respectively. The pyranometers are permanently installed south-facing. For the albedo analysis data measured from 10:00 a.m. to 6:00 p.m. LST under clear sky conditions were considered.

2.3. Sensitivity analysis

The sensitivity analysis was performed to define the impact of each proposed solution on the indoor environment thermal performance. In fact, the sensitivity analysis allows the identification of the most significant variables and strategies (high sensitivity) able to affect building performance from both technical and economical point of view [22]. Therefore, such analysis allowed to (i) compare the effectiveness of the two solutions in improving the indoor thermal conditions of the case study building by considering both the separate and combined contributions, and (ii) determine the impact of façades orientation on the thermal passive cooling effect of the cool wall painting.

In the present work, the reflectance properties of the roof and of each wall represent the input parameters (IP) of the thermal analysis multi-variant problem. The output parameter (OP) chosen for defining the sensitivity coefficient (SC) is the maximum hourly value of indoor operative temperature (T_{op}). T_{op} results are stated as a function (Eq. (2)) of the equivalent reflectance of the building coating (R^*) that represents the sole IP variable, since it influences the heat gains through the roof and, therefore, the indoor thermal comfort conditions. In fact, the additional parameters affecting

building thermal-energy performance are the same in all the considered configurations. R^* for the building coating is expressed as the combination of the equivalent reflectance of the different envelope components. The contribution of each differently oriented building surface in the whole building R^* is affected, not only by its solar reflectance capability, but also by the specific surface size and its sun view during the day. Therefore, the variable R_i^* is therefore represented by a function (Eq. (3)) of the Solar Reflectance (R_{solar}), the surface area (A), and the view factor of surface to the sky (VF) of the i -th surface. The considered view factors for the roof and the vertical walls are computed as equal to 1 and 0.5, respectively, according to the following expression Eq. (1) [23]:

$$VF_{s-sky} = 0.5 \times (1 + \cos \varphi) \quad (1)$$

with φ being the tilt angle of the surface from horizontal.

Such VF_i values are defined by assuming free field conditions to the sky, even if small obstacles are observed. Therefore, the R^* value (Eq. (3)) has to be considered as slightly overestimated.

$$T_{op,max} = f(x_1; x_2; \dots; x_n) = f(R^*) \quad (2)$$

$$R_i^* = f(R_{solar,i}; A_i; VF_i) \quad (3)$$

The differential of the OP is calculated through the equations reported in [22] by considering that each IP variable is independent from every other one. The SC expressing the IP role is obtained with (Eq. (4)), considering the maximum OP situation as the base case.

$$SC = \frac{(OP_{max} - OP_{min})/OP_{max}}{(IP_{max} - IP_{min})/IP_{max}} \quad [-] \quad (4)$$

2.4. Analytical modelling

In this section, an analytical methodology was implemented with the purpose to (i) define a T^*_{skin} surface temperature function representative of the whole case study building coating thermal behaviour and able to reproduce the difference between the standard and the cool configuration, and (ii) develop a model able to accurately predict the thermal performance of the considered building coating, based on a minimum number of surface temperature measurements in specifically selected positions on the building external surface. In particular, the T^*_{skin} temperature function is defined by taking into account the impact of the differently oriented façades, and could be a useful tool when predicting buildings behaviour by means of both numerical and analytical modelling software. The obtained external surface temperature profiles could be used, for instance, as boundary conditions in CFD modelling tools when outdoor areas are studied. Furthermore, this analytical model also defines a reference procedure that aims to minimize the experimental monitoring effort by optimizing both the number of surface temperature sensors to be used and their position on the building coating.

The proposed approach consists of the following main steps:

- selection of monitored days which are representative of summer typical weather boundary conditions (i.e. 5 days), for both the cool and standard configuration of the prototype building;
- experimental fitting of the measured surface temperature values for each building surface (i.e. North, South, East, and West façade and roof) by means of Fourier of 3rd order series;
- definition of dedicated Fourier parameters representative of all the selected summer days and of all the different orientations of the building surfaces. In this way, eight average parameters, which allow to accurately describe the local surface temperature profile, were obtained for each orientation (T^*_j);
- evaluation of the inaccuracy deriving from the use of the T^*_j surface temperature function rather than the experimental measurement for each differently oriented building surface, i.e. North, South, West, and East façade, and roof;

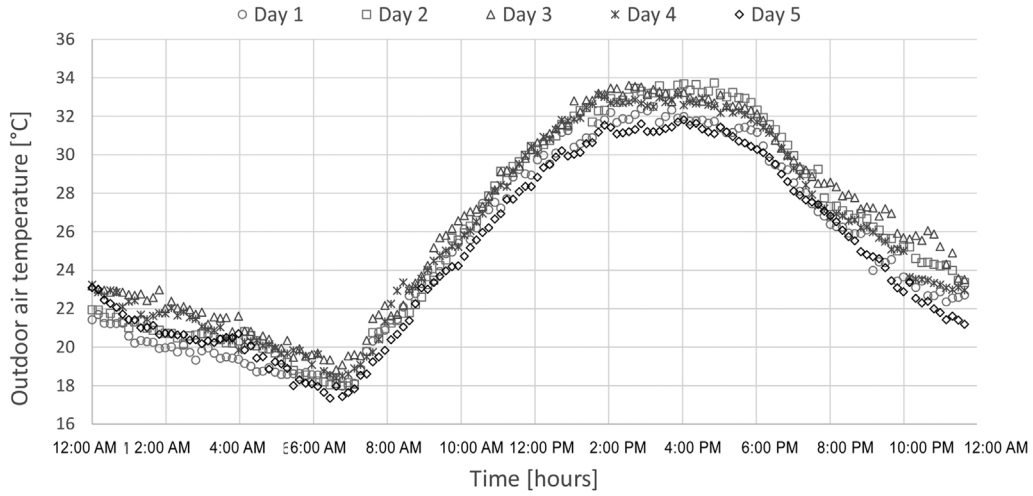


Fig. 3. Trend over time of the experimental ambient temperature values in the five summer monitored days.

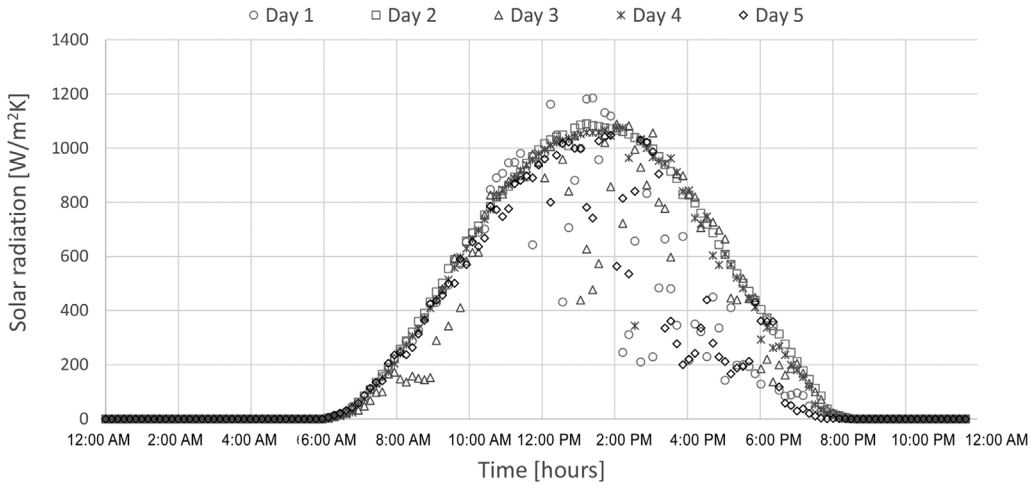


Fig. 4. Trend over time of the experimental solar radiation values in the five summer monitored days.

- definition of new Fourier parameters representative of all the selected summer days and of all the different orientations of the building surfaces. In this way, eight average parameters, which can be used to define a single T_{skin}^* surface temperature function describing the thermal behavior of the whole case study building without neglecting the impact of different surface orientations, were obtained by considering all the 5 selected typical summer days;
- validation of the implemented model by extending the achieved results to additional summer days characterized by different weather boundary conditions in terms of dry-bulb temperature, mainly.

Therefore, after collecting the available experimental data, a curve fitting was carried out by taking into account the five outdoor surface temperature profiles of the envelope components in five monitored days selected as to be representative of typical summer conditions in terms of both ambient temperature and solar radiation (Figs. 3 and 4).

A Fourier series of 3rd order was found to be the function able to better approximate the series of the collected data with the minimum number of parameters, for both the standard and cool scenario, since calculated r^2 values were always above 0.96 (Eqs. (5)–(9)):

$$T_{ei} = e_{1i} + e_{2i} \cos(e_{8i}x) + e_{3i} \sin(e_{8i}x) + e_{4i} \cos(e_{8i}2x) + e_{5i} \sin(e_{8i}2x) + e_{6i} \cos(e_{8i}3x) + e_{7i} \sin(e_{8i}3x) \quad (5)$$

$$T_{wi} = w_{1i} + w_{2i} \cos(w_{8i}x) + w_{3i} \sin(w_{8i}x) + w_{4i} \cos(w_{8i}2x) + w_{5i} \sin(w_{8i}2x) + w_{6i} \cos(w_{8i}3x) + w_{7i} \sin(w_{8i}3x) \quad (6)$$

$$T_{si} = s_{1i} + s_{2i} \cos(s_{8i}x) + s_{3i} \sin(s_{8i}x) + s_{4i} \cos(s_{8i}2x) + s_{5i} \sin(s_{8i}2x) + s_{6i} \cos(s_{8i}3x) + s_{7i} \sin(s_{8i}3x) \quad (7)$$

$$T_{ni} = n_{1i} + n_{2i} \cos(n_{8i}x) + n_{3i} \sin(n_{8i}x) + n_{4i} \cos(n_{8i}2x) + n_{5i} \sin(n_{8i}2x) + n_{6i} \cos(n_{8i}3x) + n_{7i} \sin(n_{8i}3x) \quad (8)$$

$$T_{ri} = r_{1i} + r_{2i} \cos(r_{8i}x) + r_{3i} \sin(r_{8i}x) + r_{4i} \cos(r_{8i}2x) + r_{5i} \sin(r_{8i}2x) + r_{6i} \cos(r_{8i}3x) + r_{7i} \sin(r_{8i}3x) \quad (9)$$

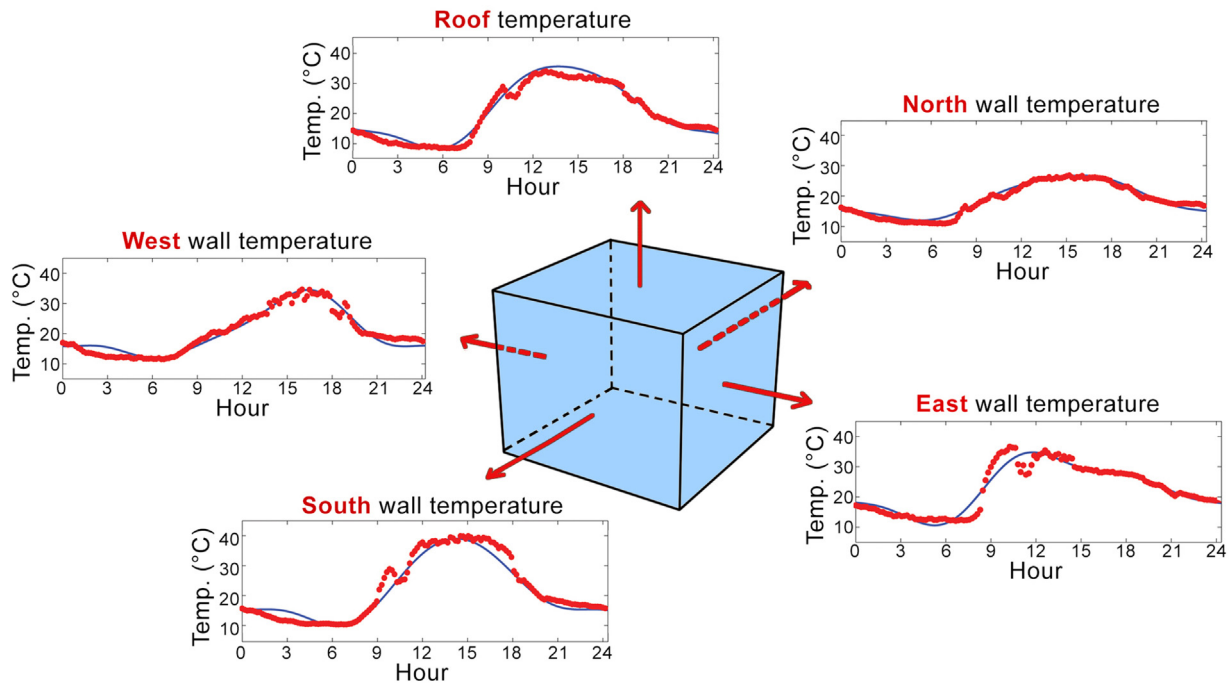


Fig. 5. Building thermal profiles of each differently oriented coating surface generated by means of the implemented analytical tool.

With e_i , w_i , n_i , s_i , r_i , being the Fourier series fitting coefficients for each specific coating surface, and i being the number of the selected day, varying between 1 and 5.

Since the selected analytical model seemed to be suitable to properly describe the thermal profile of each wall external surface (Fig. 5), the same function was assumed to be representative of the thermal behaviour of the single surface (T^*_j), and of the whole building coating (T^*_{skin}).

Therefore, the coefficients associated to each differently oriented surface, i.e. the five coefficients produced in the previously described fitting procedure (e_i , w_i , n_i , s_i , r_i , with $i = 1, \dots, 5$), were averaged in order to define a T^*_j approximated coating surface temperature function for the five orientations (i.e., north, south, east, west, and the roof), by using a function of the same kind and order, i.e. Fourier series of 3rd order (Eq. (10)):

$$T^*_j = a_{0j} + a_{1j} \cos(c_j x) + b_{1j} \sin(c_j x) + a_{2j} \cos(c_j 2x) + b_{2j} \sin(c_j 2x) + a_{3j} \cos(c_j 3x) + b_{3j} \sin(c_j 3x) \quad (10)$$

With j being the different surface orientations considered, i.e. $j = \text{east (E), west (W), south (S), north (N), roof (R)}$.

A Fourier series of 3rd order was also used to define the approximated whole building coating surface temperature T^*_{skin} (Eq. (11)). However, in this case, the Fourier parameters were defined as the average of a_{0j} , a_{1j} , a_{2j} , a_{3j} , b_{1j} , b_{2j} , b_{3j} , and c_j (from Eq. (10)), referring to the differently oriented surfaces (i.e. with $j = \text{north, south, west, east}$).

east).

$$T^*_{skin} = a_0 + a_1 \cos(cx) + b_1 \sin(cx) + a_2 \cos(c2x) + b_2 \sin(c2x) + a_3 \cos(c3x) + b_3 \sin(c3x) \quad (11)$$

While the T^*_j function, which is specific for the temperature profiles of the different surfaces, allows to determine the impact of the surface orientation on the effectiveness of the application of cool solutions, the T^*_{skin} function can be considered as representative of the thermal behaviour of the whole building coating.

Finally, the prediction capability of the implemented analytical model was extended to different summer days. To this aim, firstly the Fourier parameters of the model were normalized with respect to one selected building surface. For instance, terms normalized with respect to the east wall are shown in Table 1.

Secondly, an additional day was picked from the summer monitored period and the model was used to describe the surface temperature profile of the differently oriented surfaces. To do so, the experimentally measured temperature profile of the selected building surface, e.g. the east wall, was fitted by means of the usual Fourier series of 3rd order. In this way, the Fourier parameters of the selected surface were directly defined from experimental data.

Finally, the temperature profiles of the remaining building surfaces of the additional day were defined by multiplying the normalized parameters (Table 1), by the Fourier parameters obtained through the fitting procedure of one single surface of the additional selected day.

Table 1
Fourier coefficients normalized with respect to the East wall.

	Order 0	Order 1	Order 2	Order 3	Freq.
North wall	a_{0N}/a_{0E}	a_{1N}/a_{1E}	a_{2N}/a_{2E}	a_{3N}/a_{3E}	c_N/c_E
West wall	a_{0W}/a_{0E}	a_{1W}/a_{1E}	a_{2W}/a_{2E}	a_{3W}/a_{3E}	c_W/c_E
South wall	a_{0S}/a_{0E}	a_{1S}/a_{1E}	a_{2S}/a_{2E}	a_{3S}/a_{3E}	c_S/c_E
Roof	a_{0R}/a_{0E}	a_{1R}/a_{1E}	a_{2R}/a_{2E}	a_{3R}/a_{3E}	c_R/c_E

In this way, by considering for instance the experimental surface temperature data for the east wall (see Eq. (12)), it was possible to predict all the other temperature profiles with using Eqs. (13)–(16).

$$T_E = E_1 + E_2 \cos(E_8 x) + E_3 \sin(E_8 x) + E_4 \cos(E_8 2x) + E_5 \sin(E_8 2x) + E_6 \cos(E_8 3x) + E_7 \sin(E_8 3x) \quad (12)$$

$$T_W = E_1 \cdot \left(\frac{a_{0W}}{a_{0E}} \right) + E_2 \cdot \left(\frac{a_{1W}}{a_{1E}} \right) \cos\left(E_8 \cdot \left(\frac{c_W}{c_E} \right) x\right) + E_3 \cdot \left(\frac{b_{1W}}{b_{1E}} \right) \sin\left(E_8 \cdot \left(\frac{c_W}{c_E} \right) x\right) + E_4 \cdot \left(\frac{a_{2W}}{a_{2E}} \right) \cos\left(E_8 \cdot \left(\frac{c_W}{c_E} \right) 2x\right) + E_5 \cdot \left(\frac{b_{2W}}{b_{2E}} \right) \sin\left(E_8 \cdot \left(\frac{c_W}{c_E} \right) 2x\right) + E_6 \cdot \left(\frac{a_{3W}}{a_{3E}} \right) \cos\left(E_8 \cdot \left(\frac{c_W}{c_E} \right) 3x\right) + E_7 \cdot \left(\frac{b_{3W}}{b_{3E}} \right) \sin\left(E_8 \cdot \left(\frac{c_W}{c_E} \right) 3x\right) \quad (13)$$

$$T_S = E_1 \cdot \left(\frac{a_{0S}}{a_{0E}} \right) + E_2 \cdot \left(\frac{a_{1S}}{a_{1E}} \right) \cos\left(E_8 \cdot \left(\frac{c_S}{c_E} \right) x\right) + E_3 \cdot \left(\frac{b_{1S}}{b_{1E}} \right) \sin\left(E_8 \cdot \left(\frac{c_S}{c_E} \right) x\right) + E_4 \cdot \left(\frac{a_{2S}}{a_{2E}} \right) \cos\left(E_8 \cdot \left(\frac{c_S}{c_E} \right) 2x\right) + E_5 \cdot \left(\frac{b_{2S}}{b_{2E}} \right) \sin\left(E_8 \cdot \left(\frac{c_S}{c_E} \right) 2x\right) + E_6 \cdot \left(\frac{a_{3S}}{a_{3E}} \right) \cos\left(E_8 \cdot \left(\frac{c_S}{c_E} \right) 3x\right) + E_7 \cdot \left(\frac{b_{3S}}{b_{3E}} \right) \sin\left(E_8 \cdot \left(\frac{c_S}{c_E} \right) 3x\right) \quad (14)$$

$$T_N = E_1 \cdot \left(\frac{a_{0N}}{a_{0E}} \right) + E_2 \cdot \left(\frac{a_{1N}}{a_{1E}} \right) \cos\left(E_8 \cdot \left(\frac{c_N}{c_E} \right) x\right) + E_3 \cdot \left(\frac{b_{1N}}{b_{1E}} \right) \sin\left(E_8 \cdot \left(\frac{c_N}{c_E} \right) x\right) + E_4 \cdot \left(\frac{a_{2N}}{a_{2E}} \right) \cos\left(E_8 \cdot \left(\frac{c_N}{c_E} \right) 2x\right) + E_5 \cdot \left(\frac{b_{2N}}{b_{2E}} \right) \sin\left(E_8 \cdot \left(\frac{c_N}{c_E} \right) 2x\right) + E_6 \cdot \left(\frac{a_{3N}}{a_{3E}} \right) \cos\left(E_8 \cdot \left(\frac{c_N}{c_E} \right) 3x\right) + E_7 \cdot \left(\frac{b_{3N}}{b_{3E}} \right) \sin\left(E_8 \cdot \left(\frac{c_N}{c_E} \right) 3x\right) \quad (15)$$

$$T_R = E_1 \cdot \left(\frac{a_{0R}}{a_{0E}} \right) + E_2 \cdot \left(\frac{a_{1R}}{a_{1E}} \right) \cos\left(E_8 \cdot \left(\frac{c_R}{c_E} \right) x\right) + E_3 \cdot \left(\frac{b_{1R}}{b_{1E}} \right) \sin\left(E_8 \cdot \left(\frac{c_R}{c_E} \right) x\right) + E_4 \cdot \left(\frac{a_{2R}}{a_{2E}} \right) \cos\left(E_8 \cdot \left(\frac{c_R}{c_E} \right) 2x\right) + E_5 \cdot \left(\frac{b_{2R}}{b_{2E}} \right) \sin\left(E_8 \cdot \left(\frac{c_R}{c_E} \right) 2x\right) + E_6 \cdot \left(\frac{a_{3R}}{a_{3E}} \right) \cos\left(E_8 \cdot \left(\frac{c_R}{c_E} \right) 3x\right) + E_7 \cdot \left(\frac{b_{3R}}{b_{3E}} \right) \sin\left(E_8 \cdot \left(\frac{c_R}{c_E} \right) 3x\right) \quad (16)$$

Where $E_{1...8}$ are the parameters obtained from the fitting procedure by using the Fourier of 3rd order for the additional monitored summer day selected.

Similarly, by fitting the measurements for the other building external surfaces it was possible to accurately derive the temperature profile of the remaining walls and roof with no needs of additional experimental measurements.

At this point, the accuracy of the model prediction was also estimated by computing the difference between the experimentally measured data and the predicted temperature profiles. Moreover, the time interval during which the prediction capability of the model can be considered as acceptable was defined by taking into account the solar position with respect to each differently oriented building surfaces in the selected summer day. This is because the reliability of the model implemented is strongly affected by the impact of the direct solar radiation on the building surfaces, which varies for the different surfaces orientation during the day (Fig. 6a). Therefore, in order to define the appropriate time interval during which the model can accurately predict the building thermal behaviour starting from the experimental data of a single building wall, a geometrical analysis was performed by considering a Cartesian coordinate system with origin at the centre of the building base. In particular, different critical “boundary” azimuth and altitude angles were defined for each differently oriented building surface (see Eqs. (17)–(19)), by identifying the upper and lower “limit” in which the direct solar radiation is able to reach each building surface (Fig. 6b).

$$z_{lim,1} = \frac{\pi}{2} + \arcsin\left(\frac{L_e}{2r_{base}}\right) \quad (17)$$

$$z_{lim,2} = \pi + \arcsin\left(\frac{L_s}{2r_{base}}\right) \quad (18)$$

$$h_{lim} = \arcsin\left(\frac{h}{r_h}\right) \quad (19)$$

Where $z_{lim,1}$ and $z_{lim,2}$ are the boundary solar azimuth angles (upper and lower limit, respectively), h_{lim} is the boundary solar altitude angle, L_e and L_s are the East and South wall length, r_{base} is the semi-diagonal of the building base and r_h is the maximum distance between the center of the case study building and its roof.

The angular intervals, corresponding to specific timeframes, where the inaccuracy of the model in predicting the thermal profile

of each building surface is acceptable are summarized in Table 2 for each differently oriented surface.

By running the above explained model for each wall, it is possible to define how many walls it is necessary to measure in order to accurately predict the global thermal behaviour of the building.

3. Description of the case study building

The case study building consists of a fully instrumented test-room ($3.78 \times 4.00 \times 2.85$ m) situated in Perugia (Italy), and built following recent construction techniques [20]. The reference building has a rectangular double shutter window with wood frames in the South façade and a rectangular armoured door in the North façade, for a global fenestration ratio of about 0.041. The opaque envelope of the case study building was developed by using an innovative construction stratigraphy, in order to be consistent with the Italian regulations in terms of walls thermal stationary properties, and representative of a common residential building in Italy.

Table 2

Angular intervals identifying the limits of applicability of the model for each building surface based on the solar position and on the impact of direct solar radiation on each surface.

Surface orientation	Azimuth angle boundaries	Altitude angle boundaries
EAST	$z > z_{lim,1}$	$h > h_{lim}$
NORTH*	–	–
SOUTH	$z < z_{lim,1}$ OR $z > z_{lim,2}$	$h > h_{lim}$
WEST	$z < z_{lim,2}$	$h > h_{lim}$
ROOF	–	$h < h_{lim}$

* the North wall is never reached by direct solar radiation; therefore, the model is always accurate.

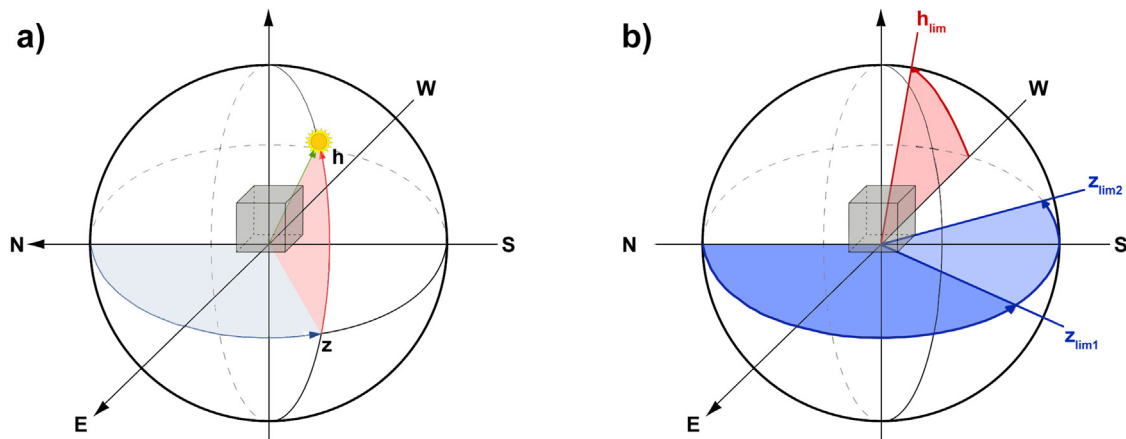


Fig. 6. (a) Directional impact of direct solar radiation on the differently oriented building coating surfaces and (b) boundary limit solar azimuth and altitude angles defined for the study.

Table 3
Thermal and morphological characterization of the case study building envelope.

	Opaque envelope properties	Layer materials (from outside to inside)
Ground floor external wall	Measured thermal transmittance = $0.59 \text{ W/m}^2 \text{ K}$ Internal heat capacity = $138 \text{ kJ/m}^2 \text{ K}$	1. Sedimentary rock: 0.12 m 2. Plaster dense: 0.04 m 3. Aerated concrete block: 0.32 m 4. Gypsum Plaster: 0.02 m
First floor external wall	Measured thermal transmittance = $1.19 \text{ W/m}^2 \text{ K}$ Internal heat capacity = $209 \text{ kJ/m}^2 \text{ K}$	1. Plaster dense: 0.02 m 2. Brickwork (Outer leaf): 0.12 m 3. Air gap: 0.05 m 4. Concrete block: 0.30 m 5. Gypsum plaster: 0.015 m
Attic external wall	Measured thermal transmittance = $0.74 \text{ W/m}^2 \text{ K}$ Internal heat capacity = $79.15 \text{ kJ/m}^2 \text{ K}$	1. Plaster dense: 0.02 m 2. Tuff (volcanic stone) brick: 0.18 m 3. Gypsum plaster: 0.015 m
Roof	Measured thermal transmittance = $1.143 \text{ W/m}^2 \text{ K}$ Internal heat capacity = $129.64 \text{ kJ/m}^2 \text{ K}$	1. Brick tiles: 0.02 m 2. Aerated concrete slab: 0.05 m 3. Brickwork (outer leaf): 0.05 m

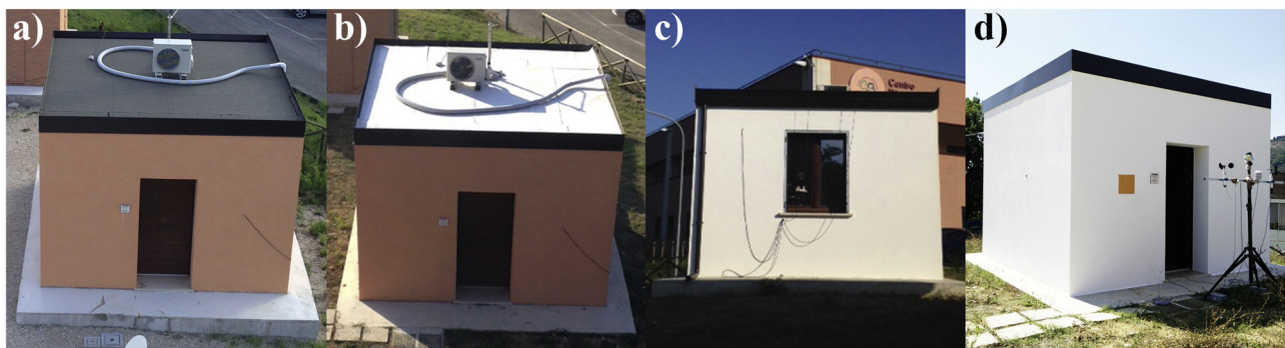


Fig. 7. Case study building in the (a) "S" configuration, (b) "CR" configuration; (c) "CR + CSF" configuration, and (d) "CE" configuration.

The specific characteristics of the test-room envelope components are specified in Table 3.

Fig. 7 reports the pictures of the roof and the façades of the case study building before (Fig. 7a) and after (Fig. 7b–d) the application of the cool membrane and reflective painting, which are acknowledged to affect building envelope thermal-energy performance [24].

The experimental setup [20] is composed by (i) an outdoor meteorological station located over the roof of the university building, close to the test-room facility, and (ii) an indoor station positioned inside the same test-room. The outdoor meteorological station allows the continuous monitoring of the main meteorological parameters, i.e. dry bulb temperature, relative humidity, wind velocity and direction, rain fall, and solar radiation. Moreover, an additional monitoring station positioned inside the prototype

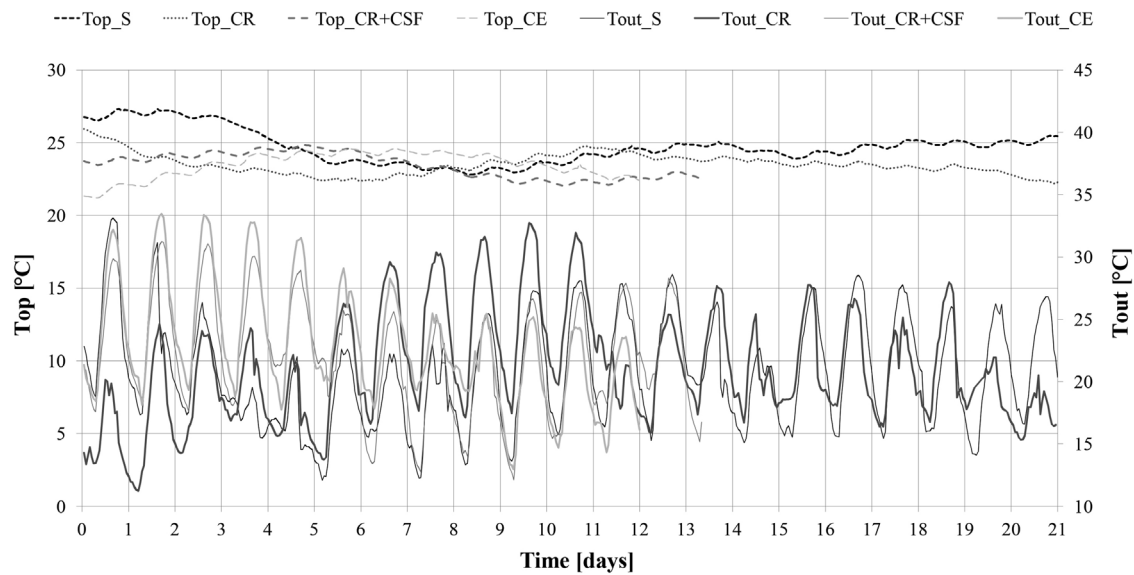


Fig. 8. Trend of indoor operative temperature with respect to outdoor dry-bulb temperature for the “S”, “CR”, “CR + CSF”, and “CE” scenarios during each monitored summer period.

building is able to measure the main thermal-energy parameters in the prototype building, i.e. walls and ceiling indoor and outdoor surface temperatures, air temperature, mean radiant temperature, relative humidity, energy consumption, etc., and the reflected radiation from the roof for the in-field measurements of albedo. Detailed information is reported in a previous work by the same authors [20].

4. Analysis of the results

4.1. Albedo field measurement

The comparison between the black bituminous membrane and the cool membrane highlights the higher solar reflectance of the innovative cool membrane. Although the average albedo measured during the monitoring period for the proposed membrane is equal to 0.51, the albedo increases by about 80% if compared to the bitumen membrane (0.11). Such increased albedo results represent an improved shield to the heat gains through the roof, as thoroughly expressed in the following analyses.

4.2. Thermal performance of the case study building

4.2.1. Cool roof effect

Further analyses were performed on the influence of the implemented cool solutions on the indoor/outdoor thermal characteristics of the test-room, i.e. indoor operative temperature and indoor and outdoor surface temperature.

The results show that with equivalent outdoor air temperature conditions the cool roofing membrane can decrease the indoor operative temperature of the prototype building by a maximum of 2.6 °C in the hottest day. Moreover, a maximum reduction of the outdoor and indoor surface temperature of the roof equal to 19.8 °C and 3.4 °C, respectively, is directly attributable to the application of the cool membrane. Therefore, the passive cooling potential of the cool roof membrane is globally significant. This has a huge impact not only in terms of improvement of the building indoor thermal conditions, but also, more widely, on the mitigation of the local environment and urban context. In fact, such cool roofing membrane can generate a local environmental benefit also in terms of UHI mitigation and CO₂ emissions offset, especially if applied not only on the roof but also in other surrounding surfaces.

4.2.2. Effect of the cool painting on the South-facing façade

The further application of the cool painting on the South-facing façade of the test-room (CR + CSF scenario) generates a lower reduction in the indoor operative temperature, i.e. 0.5 °C. Consistent and slightly lower differences are registered in terms of mean radiant temperature decrease in the CR + CSF configuration if compared to the S scenario. Whereas, the effect due to the cool façade painting is reduced when applied together with an already effective solution, i.e. cool roof.

A considerable reduction of the surface temperature is measured after the application of the cool façade painting on the South-facing façade. It is, indeed, able to reduce both the external and internal surface temperature of the South-facing wall up to 9.9 °C and 4.4 °C, respectively.

Finally, the combined effect of the cool painting and cool roofing membrane generates a maximum indoor passive cooling effect of 3.1 °C in terms of indoor operative temperature. Therefore, the combination of such passive cooling technologies could generate important thermal benefits also in terms of local UHI mitigation and improvement of the thermal conditions of the surrounding environment, since they significantly contribute to the lowering of ambient air temperatures and built surface temperatures.

4.2.3. Effect of the cool painting over the whole building envelope

The application of the cool façade painting also on the test-room East, West, and North-facing façade is able to generate, as expected, a further passive cooling contribution of the indoor environment of the case study prototype building.

Figs. 8 and 9, show the indoor operative temperature trend and distribution, respectively, with respect to the outdoor dry-bulb temperature in the different investigated envelope coating configurations during each monitored summer period. In detail, the application of the cool painting (on the walls) and the cool membrane (on the roof) on the whole building envelope, i.e. “CE” configuration, is able to produce a maximum reduction in terms of indoor operative temperature of 4.4 °C compared to the standard scenario, i.e. “S”, of 1.8 °C compared to the cool roof configuration, i.e. “CR”, and of 1.3 °C with respect to the cool roof and cool South wall scenario, i.e. “CR + CSF”. The above mentioned values are calculated considering the data monitored in the hottest day for each configuration, with equivalent outdoor air temperature peak.

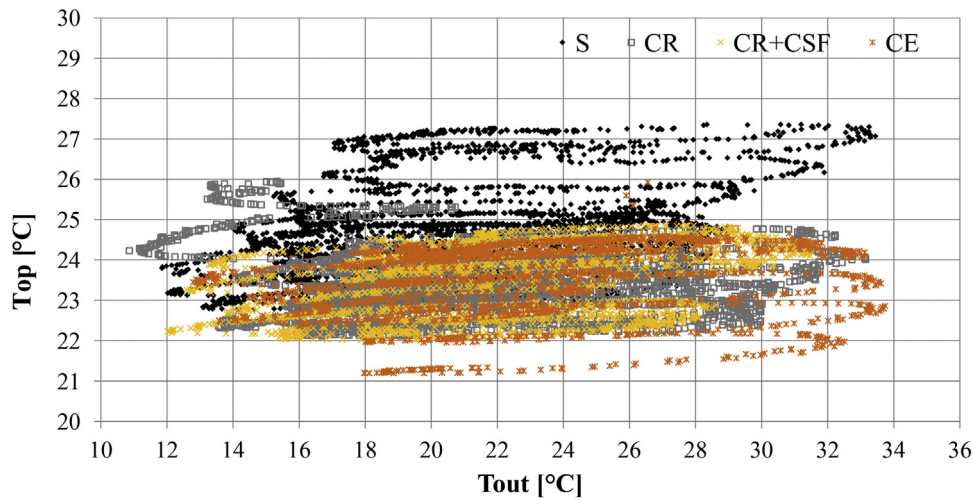


Fig. 9. Distribution of indoor operative temperature vs. outdoor dry-bulb temperature for the “S”, “CR”, “CR + CSF”, and “CE”, scenarios during the monitored summer period.

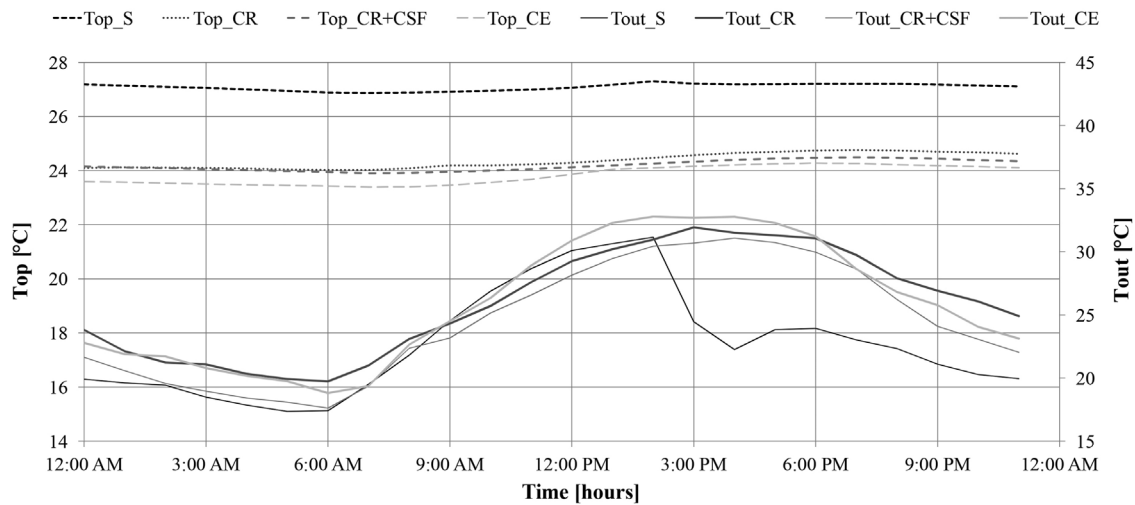


Fig. 10. Trend of indoor operative temperature with respect to outdoor dry-bulb temperature for the “S”, “CR”, “CR + CSF”, and “CE” scenarios during one summer day.

Moreover, Fig. 10 depicts the trend of indoor operative temperature with respect to outdoor air temperature during one summer day selected for each scenario in order to have similar outdoor boundary conditions in terms of air temperature and solar radiation. The daily analysis is shown to be consistent with previous results. In detail, a maximum difference of 2.6°C is measured in terms of indoor operative temperature between the standard and cool roof scenario. Additionally, a global discrepancy of 2.9 and 3.1°C is registered by considering the further application of the cool painting on the South-facing façade and on the whole building coating, respectively. Therefore, the passive cooling contribution to the improvement of the indoor thermal comfort of the prototype building directly attributable to the application of the high-albedo painting on the South-facing façade is equal to 0.3°C compared to the cool roof scenario. A further reduction of 0.5°C of the indoor operative temperature is found out for the selected day after the application of the cool painting also on the other façades, always with reference to the cool roof configuration.

4.2.4. Effect of the façade orientation

Fig. 11 shows the trend of the outdoor wall surface temperature normalized with respect to the external air temperature for each

building wall, i.e. South, North, East, and West, before and after the application of the cool wall painting.

It is evident from the graphs how the application of the innovative cool painting on the external surface of each wall is able to significantly reduce each wall surface temperature. In fact, the passive cooling effect is measured to be up to 9.9°C , 8.7°C , 13.8°C , and 11.4°C for the South, North, East, and West wall, respectively.

Additionally, it is possible to assess how the minimization of the radiative forcing is different with reference to each wall, mainly due to the different orientation and view factor. This has important implications in terms of thermal mitigation of the local urban context, since the reduction of the surface temperature leads to a globally more comfortable thermal condition of the surrounding urban environment. This has several positive implications not only in terms of thermal comfort conditions of pedestrians and urban citizens, but also more in general in terms of global energy balance and local microclimate mitigation.

Moreover, the graphs in Fig. 6 show how the correlation between the wall surface temperatures and the outdoor air temperatures is higher for the North wall, due to the stronger impact of the diffuse solar radiation component with respect to the South wall, where the hysteresis cycle is visible due to the impact of the direct radiation.

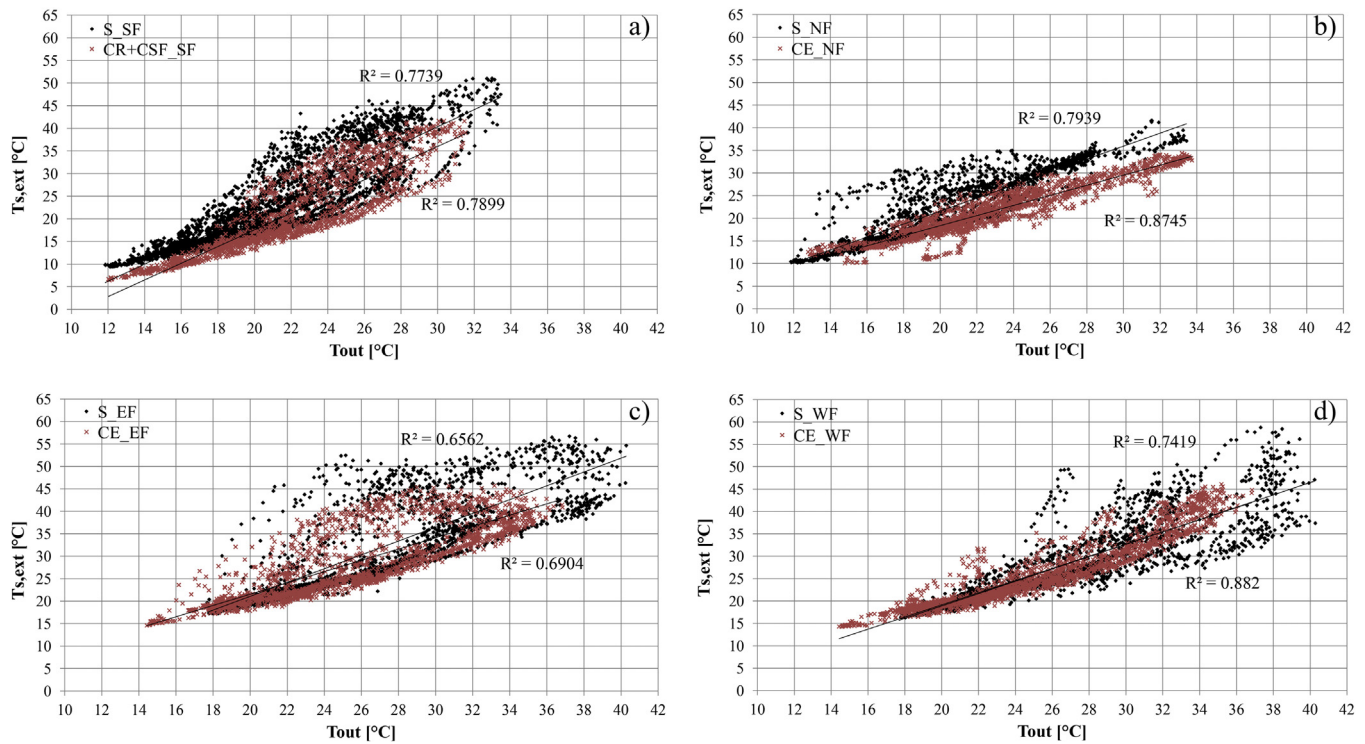


Fig. 11. Distribution of external surface temperature for the (a) South, (b) North, (c) East, and (d) West façades before (black) and after (red) the application of the cool wall painting. (For interpretation of the references to colour in this figure legend, the reader is referred to the web version of this article.)

4.3. Sensitivity analysis

The sensitivity analysis is carried out to compare the effect of the two cool coating solutions and of their coupling on the indoor thermal conditions of the case study building, also with reference to the effect of the different façade orientation. To this aim, the equivalent reflectance of the building coating is assumed as the only IP. The S scenario corresponds to the lower solar reflectance value, the CR scenario to the low-medium one, the CR + CSF scenario the high-medium one, while the CE scenario presents the higher reflectance. Fig. 12 reports the results in terms of maximum hourly value of indoor operative temperature, the OP, during the whole monitoring period.

Findings are consistent with the above-mentioned results of indoor thermal behavior. In fact, the graph indicates the effectiveness of the cool roof membrane in reducing the maximum indoor operative temperature measured, stressed by the high slope of the line between the S and the CR scenario. Moreover, the lower line slope between the CR and the CR + CSF scenario confirms the minor contribution of the cool façade painting in terms of indoor passive cooling. Finally, the application of the cool painting also on the other building façade is able to generate a further passive cooling contribution which still remains less significant with respect to the only cool roof effect.

Therefore, the two coupled coating solutions best optimize the thermal performance of the case study building. Nonetheless, the comparison among CR/CR + CSF and CR + CSF/CE results shows limited discrepancies in terms of indoor thermal comfort.

4.4. Analytical approach

Figs. 13–17 show (i) the polynomial fitting of the differently oriented building surface temperature profiles and (ii) the final averaged model for every orientation (East, South, West, North and Roof). Furthermore, the “global” surface temperature repre-

sentative of the whole case study building thermal behavior is also plotted for the cool painting scenario. Similar profiles are also obtained when the traditional painting scenario is considered.

The values of the Fourier parameters to be included in Eqs. (5)–(11) to describe the impact of the cool and the traditional painting solutions depending on the different orientation of the envelope components are summarized in Table 4.

Such numerical coefficients allow to define the impact of the different orientation on the effectiveness of the diverse envelope coating configurations, i.e. standard and cool. In particular, given the comparable angular frequencies of the considered periodical functions, i.e. column 9, the bigger the relative difference between the amplitude parameters (column 3), the higher is the impact of the cool painting and cool membrane effect on the building thermal behavior due to the orientation of each envelope surface. In fact, all the considered façades and the average coating surface temperature are associated to larger 2-coefficient values for the standard scenario with respect to the cool one. Furthermore, also the constant Fourier parameter (column 2), which can be considered as a basic temperature value for the specific building wall and whole envelope surface, generally is bigger in the standard configuration.

As a second result of this analytical assessment, the described model was used to predict the temperature profile of each building surface of a different monitored day.

Figs. 18 and 19, show the temperature profiles obtained by using the defined model while Figs. 20 and 21, show the error which is made by considering the model calibrated by means of one single temperature sensor positioned on the East and the South wall, respectively. The calibration by means of the East wall temperature sensor seems to be quite accurate for all the other building surfaces, with the exception of the South one, while obviously, by considering a thermal sensor on the South wall, the thermal profile of such surface is correctly predicted.

As a result, it can be said that by using the developed analytical model, it is possible to predict the temperature profile of each

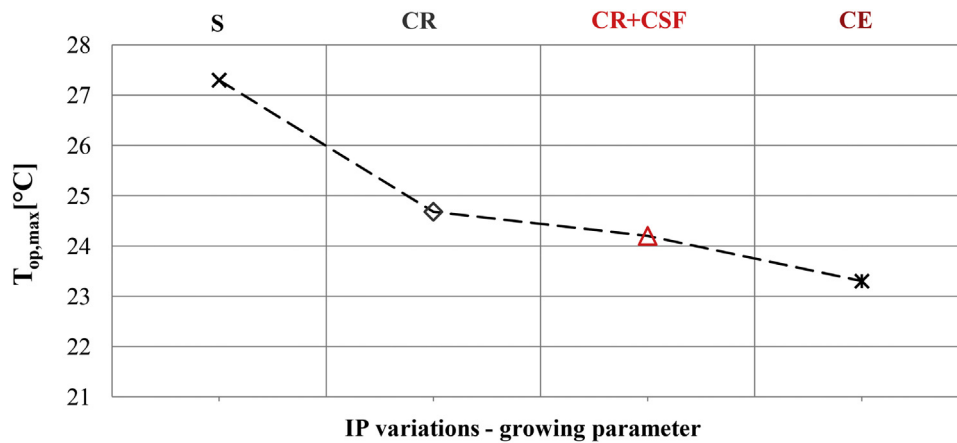


Fig. 12. Sensitivity analysis results of the effect of building coating reflectance variation on the maximum hourly value of indoor operative temperature during summer.

Table 4

Fourier coefficients of the walls temperature functions for the standard and cool roof configurations.

	Order 0	Order 1	Order 2	Order 3	Freq.
North wall	n1	n2	n3	n4	n5
STANDARD	27.498	-7.651	-6.121	-0.295	-1.504
COOL	24.396	-4.622	-6.523	0.340	1.096
East wall	e1	e2	e3	e4	e5
STANDARD	25.242	-8.484	-4.641	3.421	-2.098
COOL	29.288	-8.367	-6.911	3.291	-0.578
West wall	w1	w2	w3	w4	w5
STANDARD	27.158	-5.351	-6.183	-0.834	0.236
COOL	26.540	-2.602	-10.610	-2.179	0.754
South wall	s1	s2	s3	s4	s5
STANDARD	28.522	-11.416	-10.991	1.843	3.450
COOL	28.532	-6.370	-13.480	-0.427	2.749
Roof	r1	r2	r3	r4	r5
STANDARD	31.586	-16.666	-11.652	4.024	0.670
COOL	27.528	-8.242	-12.120	1.504	1.51
Envelope	r1	r2	r3	r4	r5
STANDARD	28.001	-9.914	-7.917	1.632	0.157
COOL	27.257	-6.041	-9.929	0.506	1.106

façade of the case study building based on a minimum number of sensors, i.e. 2, located in specifically selected positions on the building façade, i.e. East and South wall. Such forecast can be considered as accurate as long as the specific façade is not directly hit by direct solar radiation. In fact, North, East and West wall, which are shaded from the direct solar radiation for all or most of the day, are associated to highly accurate results with maximum errors of about 2 °C, while the temperature profiles of the Roof and the South surface are predicted with higher inaccuracy.

5. Discussion of the results

In this section, the main advantages and limitations of the proposed analytical approach elaborated to assess building thermal performance are discussed.

In particular, the pros of the model are as follows:

- despite the fact that the tool is case-specific, since it refers to a specific building typology and boundary conditions, the methodological procedure implemented can be easily generalized and replicated to be applied to different kind of buildings in diverse environments;
- the model is properly validated and therefore can be considered as able to accurately predict the thermal performance of the case study building for the typical summer day;

- the elaborated model allows to minimize the experimental monitoring effort in terms of (i) duration of the experimental campaign and (ii) number of monitoring sensors needed. In fact, the tool needs the experimental measurement of the surface temperature of only two envelope external surfaces out of five as input data. Moreover, a short monitoring period is needed, i.e. representative summer week. Therefore, the model could help in reducing both monitoring time and costs;
- the model is able to properly reproduce the different thermal effect of the applied coating materials, i.e. standard non-cool materials and high-albedo coatings on the indoor thermal environment of the building;
- the model could be useful (i) to define the impact of the different orientation of the building surfaces on the building coating thermal profile or (ii) to generate a univocal thermal profile for the building coating.

The main constraints and limitations of the proposed tool are listed as follows:

- even if the methodological approach can be generalized and therefore applied to other case studies, the analytical model developed in this work is case-specific, as it refers to pseudo-cubic buildings with geometrical and thermal-energy characteristics similar to those of the investigated experimental facility. Moreover, it is much related to the specific climate boundary conditions;

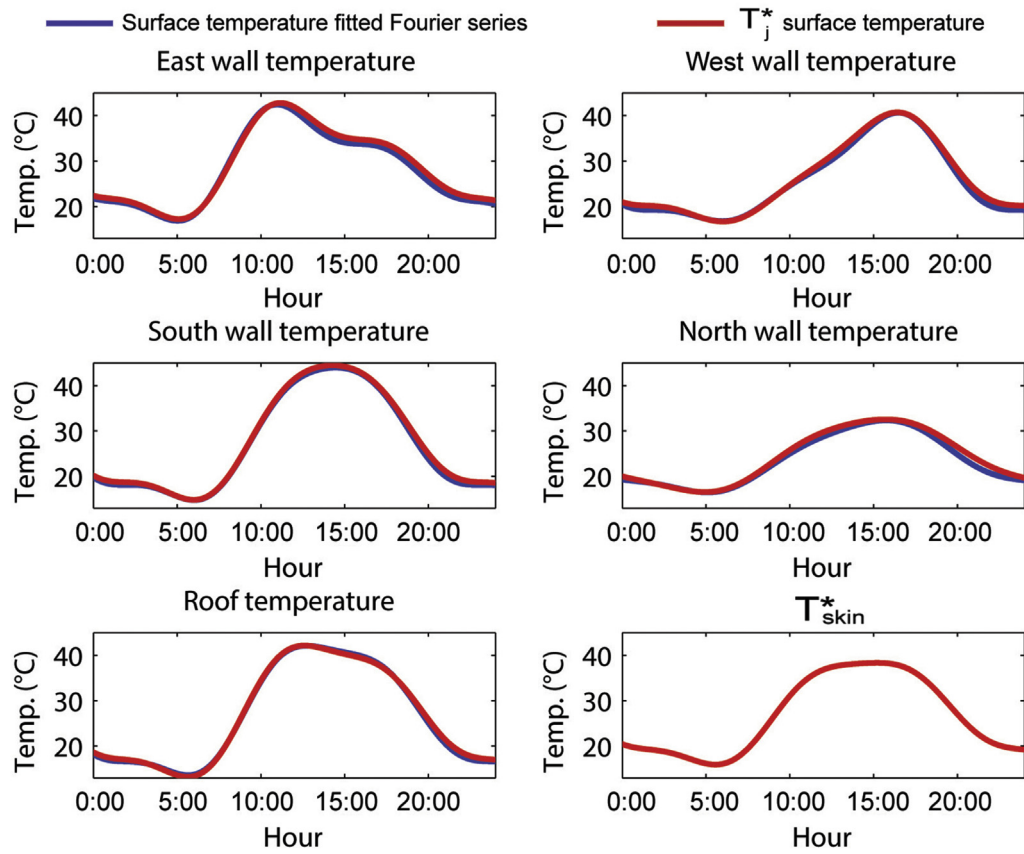


Fig. 13. Polynomial fit of the surface temperatures (day1).

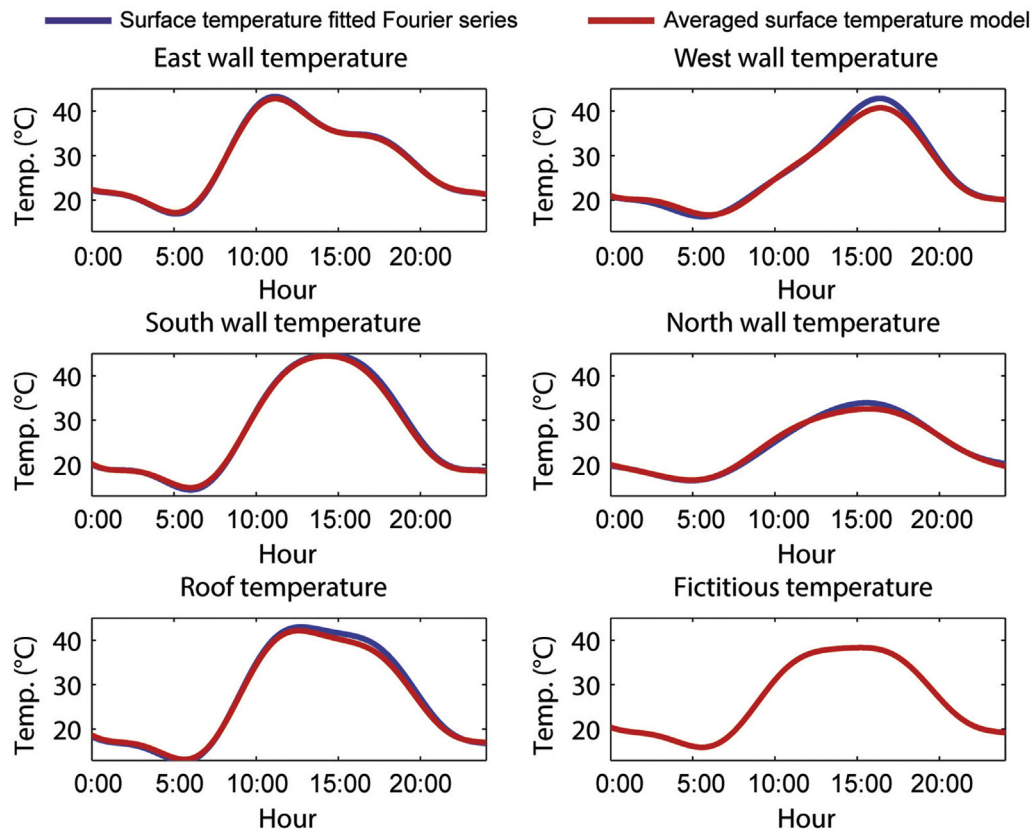


Fig. 14. Polynomial fit of the surface temperatures (day2).

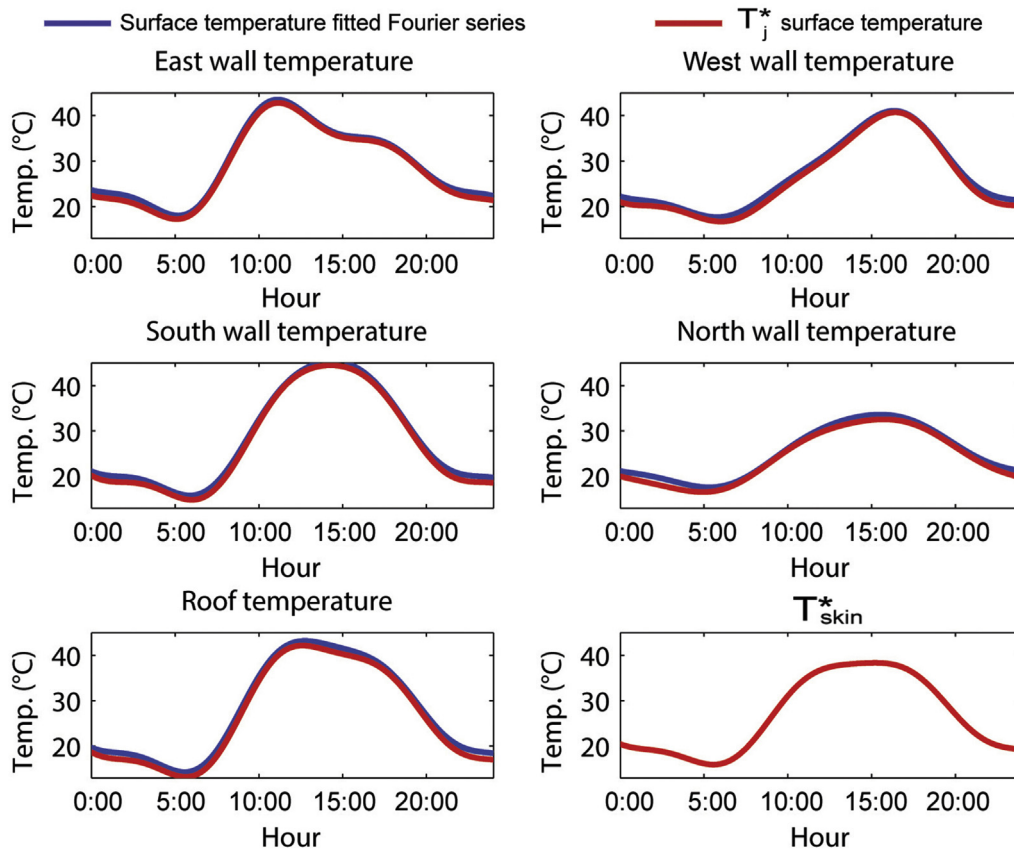


Fig. 15. Polynomial fit of the surface temperatures (day3).

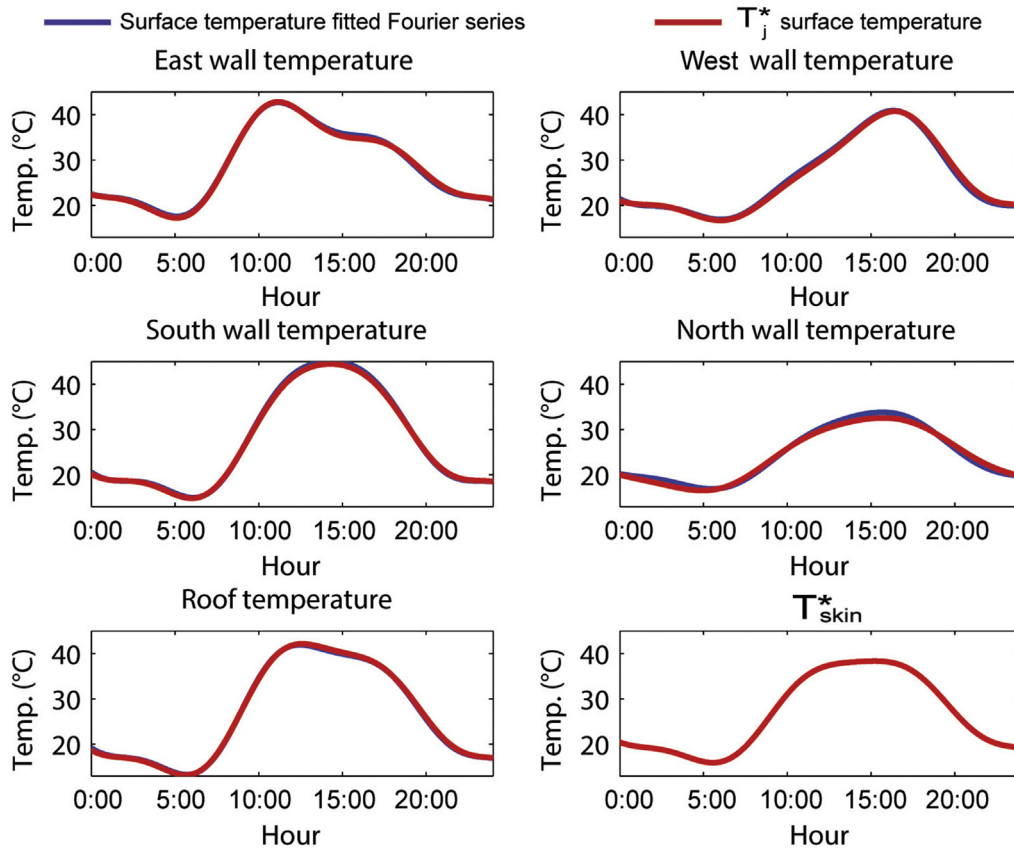


Fig. 16. Polynomial fit of the surface temperatures (day4).

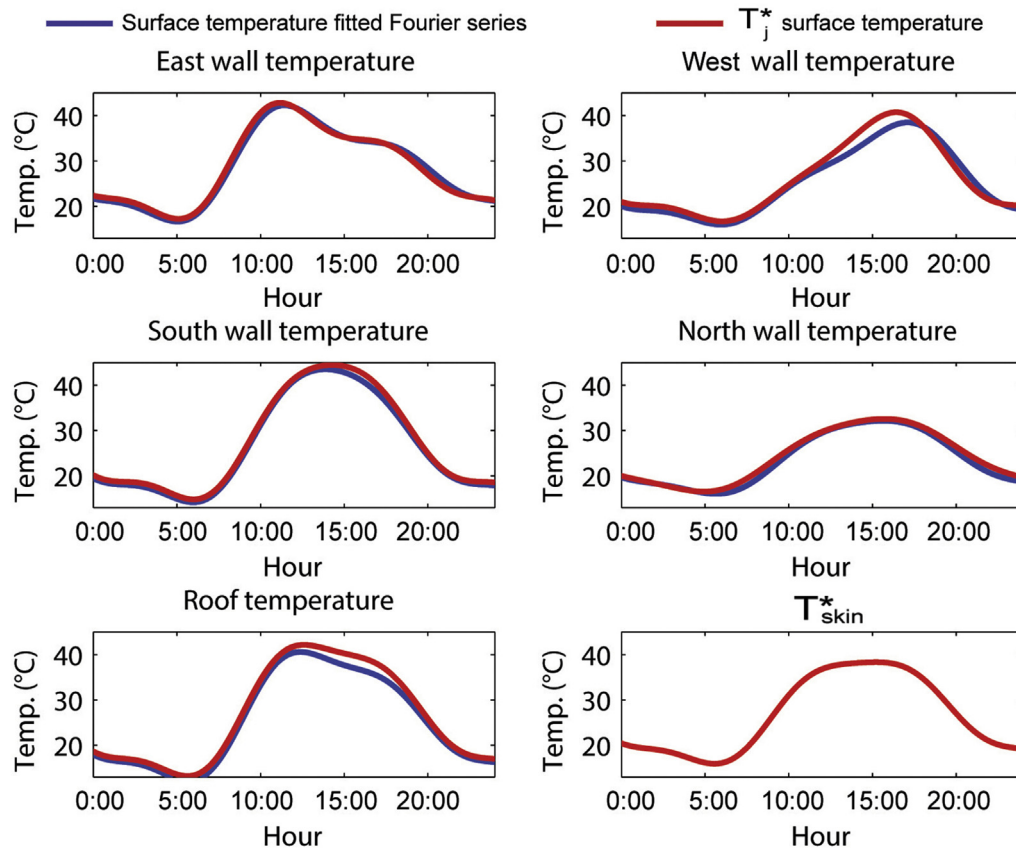


Fig. 17. Polynomial fit of the surface temperatures (day5).

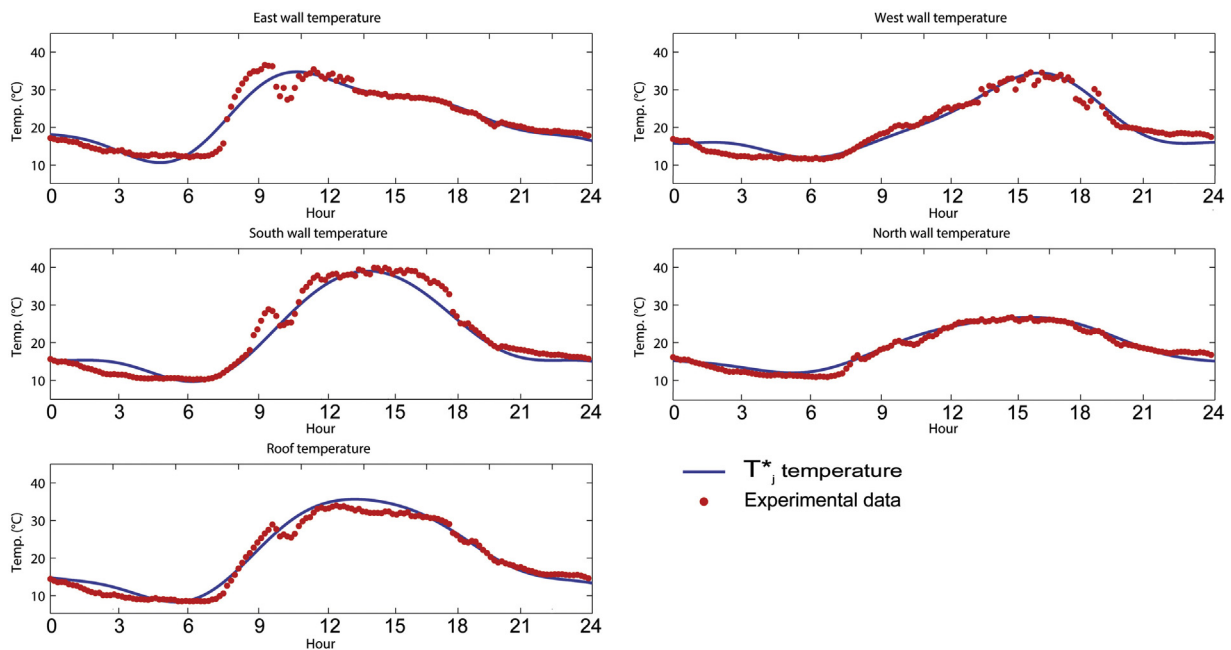


Fig. 18. Polynomial fit of the surface temperatures starting from the measured East wall surface temperature.

- the model is able to properly predict the building coating thermal behaviour only in specific identified temporal range during the day, within an acceptable error range, since it is significantly affected by the impact of the direct solar radiation;
- the reliability of the model for more complex building geometries is questionable;
- the model does not guarantee a proper prediction of the building coating thermal performance within boundary conditions that are different from the typical summer conditions evaluated in this analysis;
- the model is an empirical tool, therefore at least some experimental measurements are needed for validation purposes. After

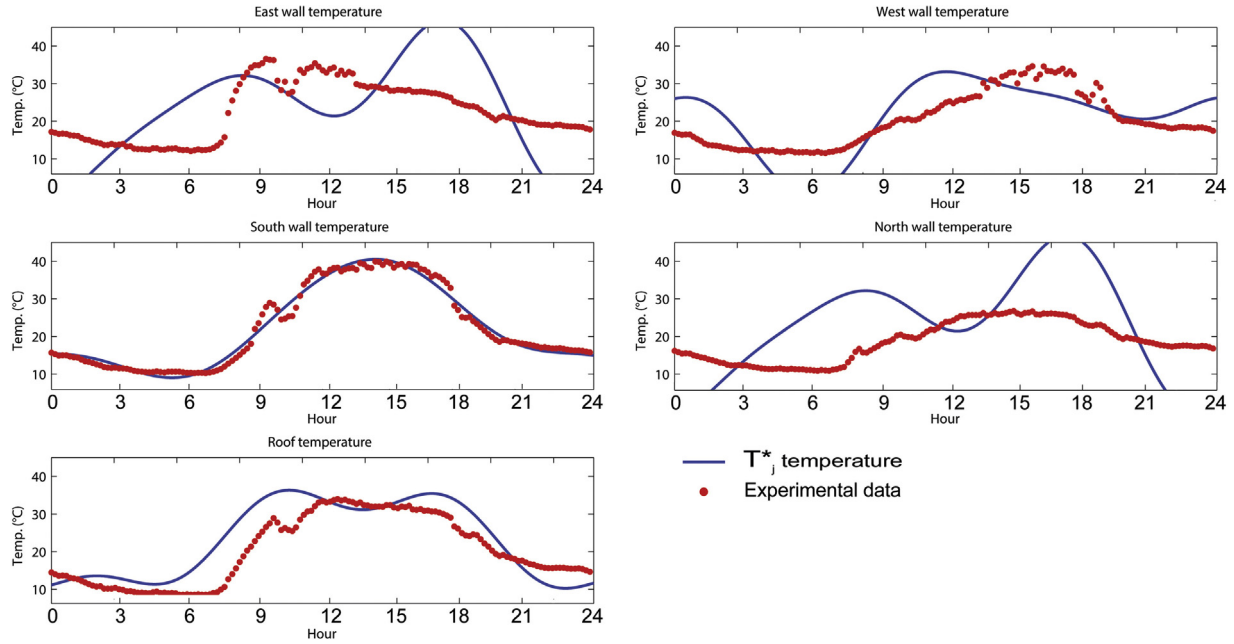


Fig. 19. Polynomial fit of the surface temperatures starting from the measured South wall surface temperature.

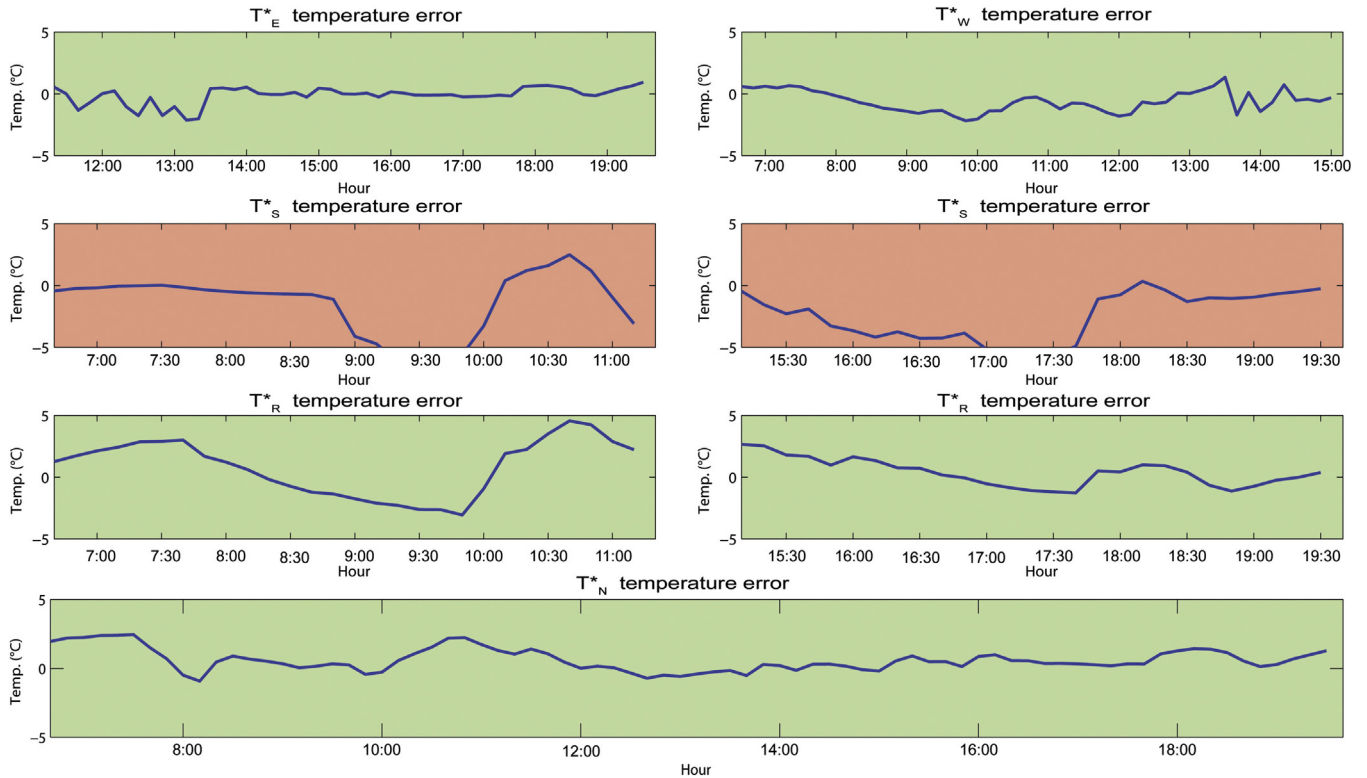


Fig. 20. Plot of the error generated in the prediction of the thermal behavior of the whole building envelope coating by measuring only the East wall surface temperature.

a preliminary continuous monitoring campaign, the number and position of the monitoring sensors can be optimized and reduced.

6. Conclusions

In this paper, experimental and analytical approaches are combined with the twofold purpose of:

- quantifying the separate and combined thermal benefits deriving from the application of cool coatings on differently oriented building envelope surfaces, i.e. wall and roof, and
- elaborating and implementing a tool to predict building external coating thermal performance with the minimum effort in terms of experimental monitoring campaign.

The results of the experimental analysis confirm a good passive cooling capability of the roof membrane, which is able to decrease up to 2.6 °C the indoor operative temperature. Moreover, the com-

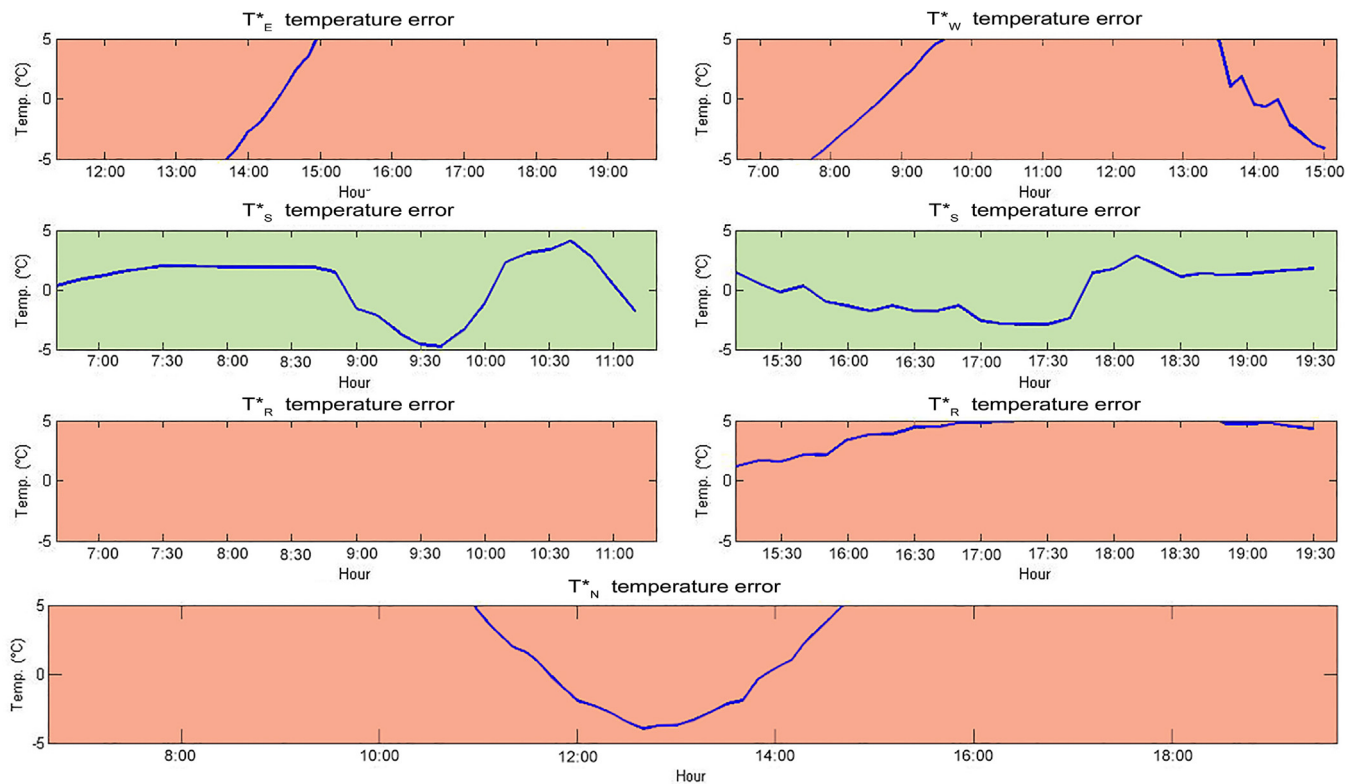


Fig. 21. Plot of the error generated in the prediction of the thermal behavior of the whole building envelope coating by measuring only the South wall surface temperature.

bination of the two cool solutions in the roof and the South-facing façade leads to an overall temperature reduction of 3.1 °C. The further application of the cool painting on the whole envelope coating produces an improvement of the indoor thermal comfort by 4.4 °C compared to the standard scenario. Even higher differences are measured in terms of surface temperatures, demonstrating how cool materials may benefit both indoor and outdoor thermal performance in summer conditions. Additionally, it is demonstrated how the passive cooling contribution of the proposed façade painting is relatively limited with respect to the cool roof effect in terms of operative temperature decrease. However, the contribution of the cool façades is considerable in terms of envelope external surface temperatures. Therefore, the findings of the experimental analysis stress how the cool façade deserves much more investigation. The possible effect in reducing building façade temperatures in urban areas, and its role in mitigating urban heat island phenomenon should be assessed more in detail, and it represents the next focus of this research.

In this view, the novel analytical procedure correctly estimates the effect of the implementation of the cool painting and membrane in terms of external surface temperature. Therefore, the analytical approach by means of Fourier series shows that the first order thermal waves for the traditional scenario presents a bigger amplitude compared to the cool scenarios, as a result of the passive cooling contribution. The analytical procedure also allows to establish that the temperature profiles of each surface of the case study building can be accurately predicted by using only two temperature sensors (i.e. in the East and South wall) and, therefore, with a key experimental effort reduction. The produced thermal profiles are in fact acceptable within a specific time interval for each surface, which is directly dependent on the amount of direct solar radiation that hits the selected surface. Therefore, the proposed analytical tool is demonstrated to effectively predict the building thermal behaviour and can be extended to all kinds of buildings, by signif-

icantly reducing experimental monitoring efforts in terms of both time and costs.

Globally, the present contribution aimed at bridging the gap between the need for extensive experimental monitoring campaigns and the prediction of external coating thermal performances, affecting outdoor microclimate in urban overheated areas. In fact, after a preliminary experimental effort and sensitivity analysis, a tool able to consistently predict any building surface temperature by minimizing the number of required experimental data has been generated. In fact, the preliminary experimental campaign presented in this work showed to be propaedeutic in order to validate and train the elaborated model and make it representative of the realistic thermal performance of façade cool coating.

Acknowledgements

The authors would like to thank the CVR s.r.l. company for providing the samples for the laboratory measurements and assisting the experimental set up. A.L. Pisello's acknowledgments are due to the UNESCO Chair "Water Resources Management and Culture", for supporting her research. The project leading to this application has received funding from the *European Union's Horizon 2020 research and innovation programme* under grant agreement No 657466 (INPATH-TES). The project leading to this application has received funding from the *European Union's Horizon 2020 research and innovation programme* under grant agreement No 678407 (ZERO-PLUS).

References

- [1] M. Santamouris, *Cooling the cities – A review of reflective and green roof mitigation technologies to fight heat island and improve comfort in urban environments*, Sol. Energy 103 (2014) 682–703.
- [2] M. Santamouris, N. Gaitani, A. Spanou, M. Saliari, K. Giannopoulou, K. Vasilakopoulou, T. Kardomateas, *Using cool paving materials to improve microclimate of urban areas – Design realization and results of the flisvos project*, Build. Environ. 53 (2012) 128–136.

- [3] A. Gros, E. Bozonnet, C. Inard, Cool materials impact at district scale – Coupling building energy and microclimate models, *Sustain. Cities Soc.* 13 (2014) 254–266.
- [4] I. Hernández-Pérez, G. Álvarez, J. Xamán, I. Zavala-Guillén, J. Arce, E. Simá, Thermal performance of reflective materials applied to exterior building components – A review, *Energy Build.* 80 (2014) 81–105.
- [5] Y. Ma, B. Zhu, K. Wu, Preparation and solar reflectance spectra of chameleon-type building coatings, *J. Sol. Energy* 70 (2001) 417–422.
- [6] C. Yu, W.N. Hien, Thermal impact of strategic landscaping in cities: a review, *Adv. Build. Energy Res.* 3 (1) (2003) 237–260.
- [7] H. Akbari, Shade trees reduce building energy use and CO₂ emissions from power plants, *Environ. Pollut.* 116 (1) (2002) 119–126.
- [8] M. Santamouris, Using cool pavements as a mitigation strategy to fight urban heat island – A review of the actual developments, *Renew. Sustain. Energy Rev.* 26 (2013) 224–240.
- [9] M. Kolokotroni, B.L. Gowreesunker, R. Giridharan, Cool roof technology in London: an experimental and modelling study, *Energy Build.* 67 (2013) 658–667.
- [10] E. Mastrapostoli, T. Karlessi, A. Pantazaras, D. Kolokotsa, K. Gobakis, M. Santamouris, On the cooling potential of cool roofs in cold climates: use of cool fluorocarbon coatings to enhance the optical properties and the energy performance of industrial buildings, *Energy Build.* 69 (2014) 417–425.
- [11] M. Doya, E. Bozonnet, F. Allard, Experimental measurement of cool facades' performance in a dense urban environment, *Energy Build.* 55 (2012) 42–50.
- [12] G.M. Revel, M. Martarelli, M. Emiliani, A. Gozalbo, M.J. Orts, M.A. Bengochea, L.G. Delgado, A. Gaki, A. Katsiapi, M. Taxiarchou, I. Arabatzis, I. Fasaki, S. Hermanns, Cool products for building envelope – Part I: Development and lab scale testing, *Sol. Energy* 105 (2014) 770–779.
- [13] G.M. Revel, M. Martarelli, M. Emiliani, L. Celotti, R. Nadalini, A. De Ferrari, S. Hermanns, E. Beckers, Cool products for building envelope – Part II: Experimental and numerical evaluation of thermal performances, *Sol. Energy* 105 (2014) 780–791.
- [14] I. Farrou, M. Kolokotroni, M. Santamouris, Building envelope design for climate change mitigation: a case study of hotels in Greece, *Int. J. Sus. Energy* 35–10 (2016) 944–967.
- [15] C. Georgakis, S. Zoras, M. Santamouris, Studying the effect of cool coatings in street urban canyons and its potential as a heat island mitigation technique, *Sustain. Cities Soc.* 13 (2014) 20–31.
- [16] M. Santamouris, Using cool pavements as a mitigation strategy to fight urban heat island – A review of the actual developments, *Renew. Sustain. Energy Rev.* 26 (2013) 224–240.
- [17] A.L. Pisello, V.L. Castaldo, G. Pignatta, F. Cotana, M. Santamouris, Experimental in-lab and in-field analysis of waterproof membranes for cool roof application and urban heat island mitigation, *Energy Build.* (2015), <http://dx.doi.org/10.1016/j.enbuild.2015.05.026>.
- [18] A.L. Pisello, V.L. Castaldo, C. Piselli, G. Pignatta, F. Cotana, Combined thermal effect of cool roof and cool façade on a prototype building, *Energy Procedia* 78 (2015) 1556–1561, <http://dx.doi.org/10.1016/j.egypro.2015.11.205>.
- [19] ASTM E1918 – 06 Standard Test Method for Measuring Solar Reflectance of Horizontal and Low-Sloped Surfaces in the Field.
- [20] A.L. Pisello, F. Cotana, A. Nicolini, C. Buratti, Effect of dynamic characteristics of building envelope on thermal-energy performance in winter conditions: in field experiment, *Energy Build.* 80 (2014) 218–230.
- [21] I.S.O. 9060, Solar energy—Specification and classification of instruments for measuring hemispherical solar and direct solar radiation, 1990.
- [22] A.L. Pisello, C. Piselli, F. Cotana, Influence of human behavior on cool roof effect for summer cooling, *Build. Environ.* 88 (2015) 116–128.
- [23] J. Hensen, R. Lamberts, *Building Performance Simulation for Design and Operation*, Routledge edition, 2012.
- [24] A. Synnefa, M. Santamouris, H. Akbari, Estimating the effect of using cool coatings on energy loads and thermal comfort in residential buildings in various climatic conditions, *Energy Build.* 39 (11) (2007) 1167–1174.